

Classification of Red Blood Cell Rigidity from Sequence Data of Blood Flow Simulations using Neural Networks

Katarína Bachratá ^{1*} , Katarína Buzáková ^{1*} , Michal Chovanec ², Hynek Bachratý ^{1*}, Monika Smiešková ¹  and Alžbeta Bohiniková ¹ 

¹ Department of Software Technology, Faculty of Management Science and Informatics, University of Žilina

² Tachyum, s.r.o., Bratislava, Slovakia

* Correspondence: katarina.bachrata@fri.uniza.sk (K.Ba.), katarina.jasencakova@fri.uniza.sk (K.Bu.), hynek.bachraty@fri.uniza.sk (H.B.)

Abstract: Numerical models for the flow of blood and other fluids can be used to design and optimize microfluidic devices computationally and thus to save time and resources needed for production, testing and redesigning of the physical microfluidic devices. Like biological experiments, computer simulations have their limitations. Data from both the biological and the computational experiments can be processed by machine learning methods to obtain new insights which then can be used for the optimization of the microfluidic devices and also for diagnostic purposes. In this work, we propose a method for identifying red blood cells in flow by their stiffness based on their movement data processed by neural networks. We describe the performed classification experiments and evaluate their accuracy in various modifications of the neural network model. We outline other uses of the model for processing data from video recordings of blood flow. The proposed model and neural network methodology classify healthy and more rigid (diseased) red blood cells with the accuracy of about 99.5 % depending on the selected dataset that represents the flow of a suspension of blood cells of various levels of stiffness.

Keywords: neural networks; microfluidic devices; red blood cells classification; sequential data

Citation: Bachratá, K.; Buzáková, K.; Chovanec, M.; Bachratý, H.; Smiešková, M.; Bohiniková, A. Classification of red blood cell rigidity from sequence data of blood flow simulations using neural networks. *Symmetry* **2021**, *1*, 0. <https://doi.org/>

Received:

Accepted:

Published:

Publisher's Note: MDPI stays neutral with regard to jurisdictional claims in published maps and institutional affiliations.

Copyright: © 2021 by the authors. Submitted to *Symmetry* for possible open access publication under the terms and conditions of the Creative Commons Attribution (CC BY) license (<https://creativecommons.org/licenses/by/4.0/>).

1. Introduction

Research and development in the field of microfluidics have increased significantly in recent years. One of the main focuses has been the study of the behaviour of fluids in microfluidic devices as well as the development of technologies for manufacturing such devices of various shapes, sizes and materials. The inner structure of these devices ranges from simple straight channels with few or no obstacles to complex geometric designs with a very specific use [1].

Testing real prototypes of microfluidic devices for their further improvement is often technologically demanding, expensive and time-consuming. Numerical models of blood flows offer an alternative approach. One of the main advantages is that the topology of the channel in the numerical model can be easily changed, allowing the evaluation of the behaviour of cells in the flow under various conditions. Thus, the functionality of the proposed device can be verified at a much lower cost, and only the devices with optimal design of their inner structure can be manufactured and tested. Cell in Fluid, Biomedical Modeling & Computation Group (CIF) [2] developed numerical model of RBC immersed in fluid [3]. One of the main research objectives of CIF is the optimization of the inner structure of microfluidic devices designed to capture and sort circulating tumour cells from other solid blood components [4]. These devices can be used for early diagnosis of cancer using only a blood sample. The identification and enumeration of circulating tumour cells can also help to indicate the effectiveness and suitability of the prescribed treatment. Research at CIF also focuses on other topics related to microfluidics, such as the study of red blood cell (RBC) damage occurring when the

cells pass through a microfluidic channel, or the investigation of bulk properties of dense cell suspensions in the blood flow [5,6].

Although there are many advantages to using numerical models, they are quite complex and thus require advanced hardware and extensive computational time. Especially simulations of blood suspensions with higher hematocrits. Each simulation provides a large amount of output data and usually, only a small fraction of it is used to evaluate a specific phenomenon. However, the already obtained output data can be processed with suitable statistical methods to gain more information, see [7–9]. This motivated us to further investigate and process data from the simulations using various machine learning methods.

We propose three main possible applications of machine learning in the study of blood flow simulations: verification (and possible improvement) of the previously used numerical models, design of new, faster computational models and acquisition of further results from simulation data without the performance of new simulation experiments. Machine learning is well suited for analyzing large sets of data, such as the simulation output data. The proposed machine learning models can be also used to process data from video recordings of biological experiments. However, it is more difficult to obtain suitable data from laboratory experiments than from computer simulations for several reasons: Most importantly, biomedical studies often include only information relevant to the studied topic, instead of all the information needed for precise computer simulations of these experiments. Furthermore, the presented data is often not only insufficient but also inaccurate due to high technical requirements for a high-quality video recording of the experiment.

1.1. The importance of red blood cells rigidity classification

In the diagnosis of various diseases such as sickle cell anaemia, malaria, diabetes or leukaemia, it is important to detect diseased cells in a blood sample, see [10,11]. Diseased RBCs lose their natural elasticity and become more rigid. In the study [12], it was shown that more rigid RBCs infected with malaria are pushed by the healthy RBCs to the edges of the flow. This observation was used to distinguish diseased RBCs from healthy ones by using a microfluidic device with side outlets. Diseased RBCs behave similarly to leukocytes in blood vessels with a diameter of less than 300 μm . RBCs, which are smaller in size and more deformable than leukocytes, migrate to the axial centre of the vessel due to the flow rate gradient in the vessels, while the leukocytes are pushed to the walls of the vessel. In this paper, we use a neural network model to address the problem of distinguishing RBCs with other elastic properties and determining the ratio of diseased and healthy RBCs in the blood flow. A sufficiently accurate classification model should not only be able to find diseased cells but also to determine their number in the hematocrit. This makes it possible to diagnose and determine the severity of the disease and then apply the appropriate treatment.

2. Related work

In recent years, several studies have addressed the problem of classification of blood cells from microscopic images of blood using various machine learning methods. In the [13] study, a convolutional neural network (CNN) model was used to classify 8 different shapes of RBCs suffering from sickle cell anaemia from microscopic images of RBCs. The model achieved a success rate of around 80%. Different neural network (NN) models have been used to distinguish between healthy RBCs and malaria-infected RBCs. In one of the most recent studies [14], the CNN model identified infected blood cells with an accuracy of 94.57% and classified different types of infected cells with an accuracy of 88%. In this paper, we propose a model with a classification accuracy of around 99.5%.

2.1. Linear model for the identification of more rigid blood cells

To compare the simulation model with the results of biological experiments, it is necessary to determine their differences. For example by comparing video recording of blood flow from biological experiment and simulation. We compared how the linear model identifies diseased blood cells using the cell movement dataset (obtained from the simulation outputs) and using a dataset obtained from a video recording of visualization of the same simulation. The outputs from the simulation are three-dimensional geometric data representing the position and shape of the blood cell, the outputs from the video are a two-dimensional projection of the blood cell onto the selected plane. In addition to the position of the extremal points, we also use the velocity vector at the blood cell centre of the mass. In the 3D model (simulation output), the dataset for each blood cell consists of the vectors of the maximum distance in the direction of the axes, ie v_x , v_y , v_z , and the velocity of the blood cell centre of mass vel_x , vel_y , vel_z . The fluid flow is in the direction of the x axis. In the 2D model, which represents a video recording of the experiment, we work with projections onto the xy plane or the xz plane. Since we do not work with gravity in the computational simulation model, both projections should be equivalent. This section aims to demonstrate what results can be achieved using the Principal component analysis method, and subsequently the possibilities of their improvement when using neural networks. In the specific case of a dataset with 20% of slightly damaged blood cells, we show how the results differ in the 3D and 2D cases with the linear approach. Then we show that although the simulation was symmetric in the direction of the y and z axes, the Principal components analysis gives better results when projected on the y axis than when projected on the z axis.

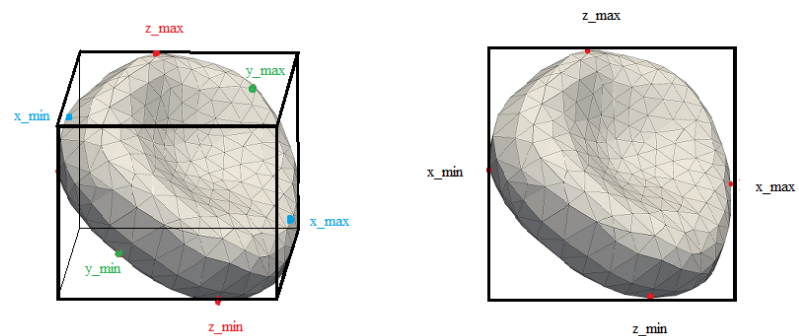


Figure 1. 3D and 2D cuboids obtained from the simulation and from the video.

In the following examination, we used data from simulation experiment *Ae20b*, which is described in section 3.1. As an input to the Principal component analysis, we used a matrix of 3D positions of extremal points and centre velocities in the direction of all three axes. In the next step, we calculated the projections of these vectors onto the planes xy and xz and calculated the distance of the vector and its projection. The average distance between the vectors and their projections serves as a boundary h , by which we distinguish between healthy and diseased blood cells. According to the rigidity of the diseased blood cells and according to the ratio of their number to the number of healthy blood cells, we multiply the value of h by an empirically determined coefficient, in our case, the coefficient is equal to 0.7.

The use of the Principal component analysis method gives us a good estimate for the effectivity of linear models. The identification of healthy and slightly damaged blood cells, the damage of which is not determinable from their geometric shape, can be made from the variance and mutual ratio of individual vectors connecting the extremal points. For blood cells in the stabilized part of the simulation, the success rate of blood cell identification is determined in Table 1.

Table 1. Identification success rate for cells from simulation of blood flow.

	Correctly identified	Incorrectly identified
Identification accuracy of diseased cells	88.99%	11.01%
Identification accuracy of healthy cells	89.51%	10.49%

125 The simplification of information in the case of the video recording of the simulation
 126 causes a reduction in accuracy. We compare the success rate of the identification in the
 127 case of simulation (i.e. three-dimensional information about cells) and in the case of
 128 video recording (two-dimensional video recording of the same simulation experiment
 129 as in Table 1). The results from the video in the case of a projection onto two different
 130 planes are in the Table 2 and Table 3.

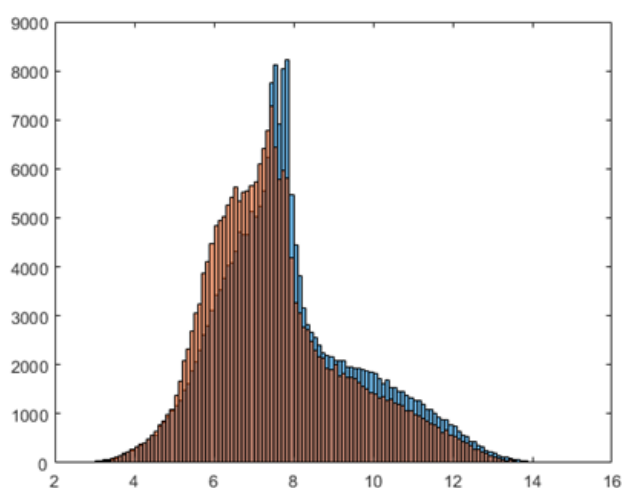
Table 2. Identification success rate for video of simulation in plane xy .

	Correctly identified	Incorrectly identified
Identification accuracy of diseased cells	86.49%	13.51%
Identification accuracy of healthy cells	77.01%	22.99%

Table 3. Identification success rate for video of simulation in plane xz .

	Correctly identified	Incorrectly identified
Identification accuracy of diseased cells	74.39%	25.61%
Identification accuracy of healthy cells	62.99%	37.01%

131 Although we expected essentially the same success rate for video recordings in
 132 the xy plane and the xz plane, the results show that simulations recorded from a "side
 133 view" have better resolution for identification of diseased blood cells than simulations
 134 recorded from the "top view". This is likely due to statistical differences between the
 135 data describing the distribution and slopes of the RBCs in the individual planes. For
 136 example in Figure 2 we see a different distribution of described cuboid side lengths in
 137 the y -axis direction and the z -axis direction. For the linear model, these differences are
 138 large enough to cause changes in the classifier performance. As we will show below,
 139 classification using neural networks is more robust and reduction to 2D case produces
 140 the same and even better results in all directions.

**Figure 2.** Distribution of described cuboid lengths in the y -axis direction (blue) and the z -axis direction (orange).

3. Materials and methods

Our method processes data describing the movement of RBCs in a simulation box. Instead of using a microscopic image of the cell as the input, we use the time sequence of its positions. This is a potential advantage when working with video data from laboratory experiments. Since these videos are often of insufficient quality, it is difficult to obtain an accurate picture of the cell. On the other hand, there are known methods for detection of the rectangular or elliptic area in which the cell is located, which can be used to describe the trajectories of RBCs, see [15,16]. Our goal is to develop a NN model which classifies RBCs by their rigidity, identifying them as healthy or diseased. The input of the model is a time sequences of positions of a given length ℓ (usually we have $\ell = 128$). The total number of positions t for a given cell differs for each simulation experiment, but in each case we have $t > \ell$, see Table A3. Our model randomly chooses a number i between 1 and $t - \ell + 1$, and then takes the sequence of ℓ consecutive positions starting at the i th position. This way some sequences might enter the model more than once, but it is faster than using all possible sequences of positions.

3.1. Description of simulation experiments

The data entering our NN model come from blood flow simulation experiments. These simulations were performed to investigate the effect of various factors, such as the ratio of healthy and diseased cells in the flow, the flow rate, or the elasticity of damaged cells, on the level of margination of diseased blood cells. Margination was formed for suspensions with a majority of healthy cells, and was more apparent in simulations with longer running times. In the used numerical model [17], the control of fluid dynamics is ensured by the lattice-Boltzmann method [18], and the elasticity of the cell membrane is controlled by the spring network model [19]. Fluid and blood cells are connected by the dissipative version of the Immersed Boundary Method (DC-IBM).

The dimensions of the simulation box are $60\mu\text{m} \times 40\mu\text{m} \times 40\mu\text{m}$, and the box does not contain any other walls or obstacles. RBCs flow in the direction of the x axis from left to right, and the channel is periodic in this direction. (This means that if a cell leaves the simulation box at one end, then it reenters it on the other end.)

The RBC model is discrete, consisting of a triangulation of the RBC surface. The modelled suspension contains 154 RBCs, each with 374 nodes. This represents a 15% hematocrit, which corresponds to the flow of blood in narrow blood vessels. We used data from 13 simulations. Individual simulations differ in the ratio of healthy and diseased RBCs, in the rigidity of diseased RBCs, and the initial location of RBCs. The rigidity of RBC is determined by its elastic parameters. Stretching coefficient k_s has the largest influence on RBC rigidity, thus we determine the rigidity of the RBCs by the value of the stretching coefficient k_s . Figure 3 shows shapes of diseased blood cells depending on the value of the stretching coefficient. In the individual experiments, all diseased RBCs had the same elastic parameters, which we list in Table A1 in appendix. Similarly, the elastic parameters of healthy RBCs (also shown in Table A1) and their mutual interactions were also the same for all experiments. The parameters of the fluid are listed in Table A2.

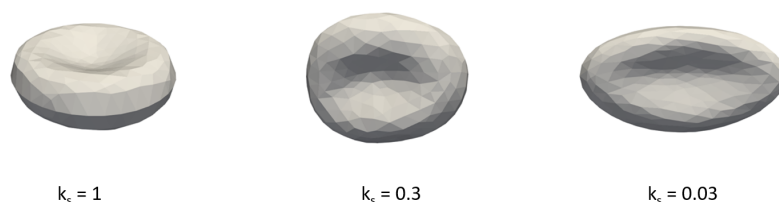


Figure 3. The elasticity of diseased RBC depending on the value of the stretching coefficient k_s .

Figure 4 shows simulated RBCs in the channel. Gray cells with $k_s = 0.005$ represent healthy RBCs, while red cells with $k_s = 0.3$ represent diseased RBCs. Table A3 shows

names of used simulations, and for each simulation we list the number of time records for a cell in the corresponding experiment. Some of the simulations are based on the previous ones. (In this case the name of the new simulation differs from the name of the original simulation only by letter *e*.) The first letter (or pair of letters) of the name of a simulation indicates the initial location of the cells. The number that follows indicates the proportion of diseased cells in the blood, and the last lower case letter indicates the rigidity of the diseased blood cells. (The letter *a* indicates the most rigid diseased blood cells ($k_s = 1$), while the letter *c* indicates the least rigid diseased blood cells ($k_s = 0.03$).)

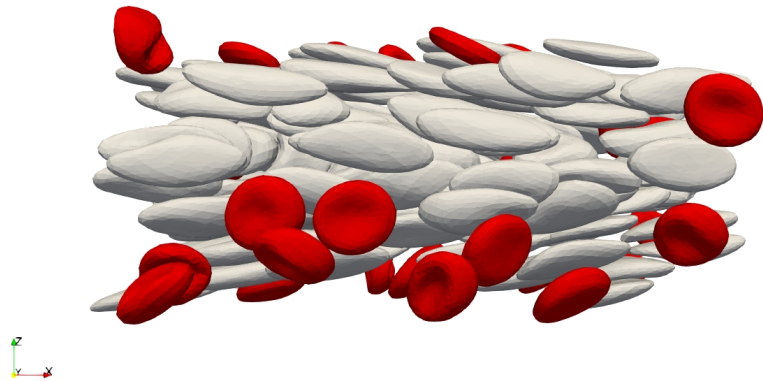


Figure 4. Cells in the simulation channel during the simulation.

3.2. Dataset and data preprocessing

The training and test data come from simulation output files in ".dat" format. We had to crop them appropriately to the shortest distance since for some simulations the number of recorded cell positions was not the same. In the classification experiments we use various simulation data about the cell movement:

- the positions of the cell centres in x , y and z direction, giving 3 data types for each RBC,
- the positions of all 6 extremal points of cells in each direction x , y and z (with or without the centre of the cell), giving either 18 or 21 data types for each RBC,
- the positions of four extremal points of cells for all 3 coordinate planes xy , xz and yz in all directions (with or without the centre of the cell), giving either 12 or 15 data types for each RBC,
- the positions of four extremal points only in the direction of the selected coordinate planes (without the centre of the cell) for all 3 coordinate planes xy , xz and yz , giving 8 data types for each RBC.

The last selection of data represents a two-dimensional image of a cell (see Figure 5 b)), from which we can easily obtain a rectangular or elliptic area in which the cell is located. The same can be done for video recordings of laboratory experiments. A sufficiently accurate model for classifying cells could thus be used to classify them from blood flow video recordings.

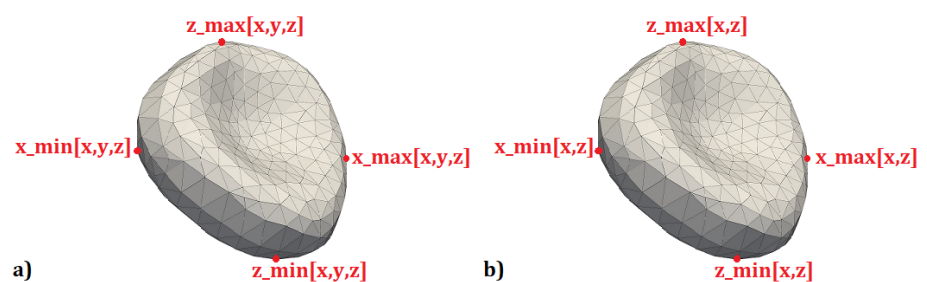


Figure 5. a) The extremal points of the cell in the xz plane in all three directions. b) The extremal points of the cell in the xz plane in the direction of the selected axes.

First, we normalized all data with an average of 0 and a variance of 1, individually for each of the 3 to 21 data types used. For a sufficiently large volume of training data, we add augmented data to the training dataset, which we create by adding a slight noise and shifting the original positions. In most experiments, we use 100 augmentations, which means that for each cell in each time step, we add 100 extra positions shifted in all directions from the original position. The size of the training dataset is

$$\sum_{i=0}^{153} (aug + 1)t_i, \quad (1)$$

where aug is the number of augmentations and t_i is the number of time records of cell movement c_i in the simulation experiment. Recall that in all experiments there are 154 cells. For example, the size of a training dataset that uses simulation data containing 700 time records of each cell's motion, and 100 augmentations, is $154 \cdot 101 \cdot 700 = 10887800$. The diagram in Figure 6 shows the classification model and dataset preprocessing.

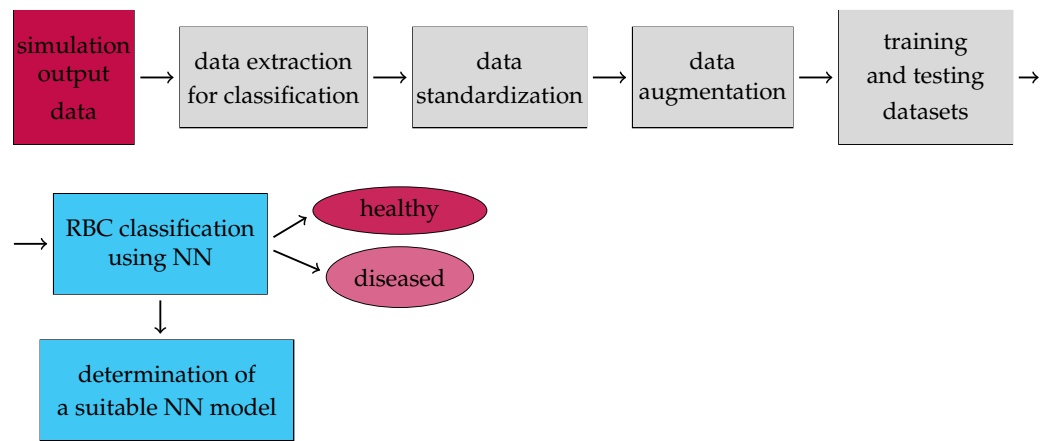


Figure 6. Flow chart of our proposed model for the classification of healthy and diseased cells in blood flow.

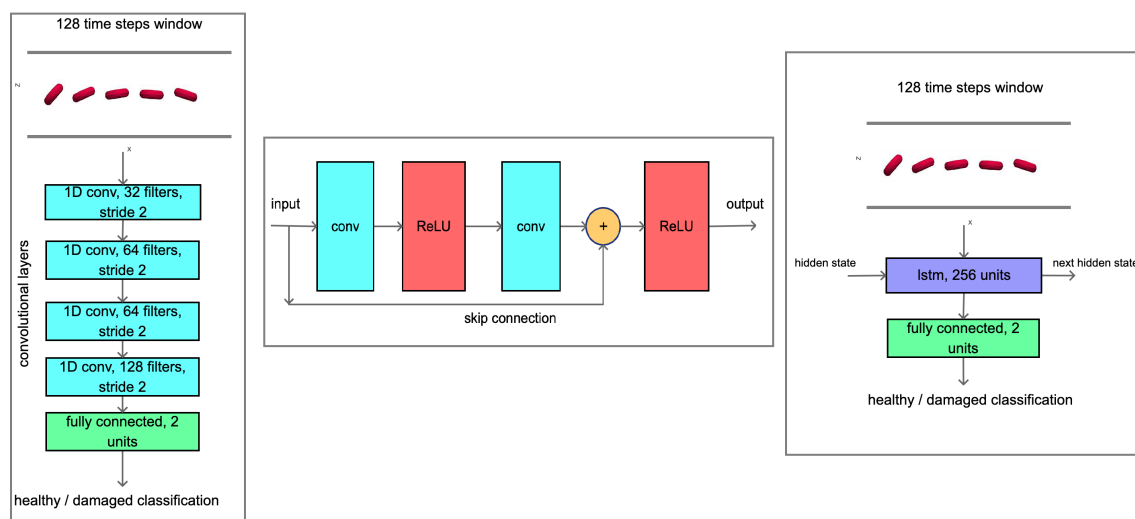
Dataset names are derived from the names of the simulation experiments in Table A3. The name of the simulation experiment whose data were used for training is followed by the name of the simulation experiment whose data were used for testing, separated by an underscore. For example, *A20a_Ae20a* is the name of a dataset that uses data from the *A20a* simulation for training and data from the *Ae20a* simulation for testing.

3.3. Tested network architectures for RBC rigidity classification

We used 22 different models of neural network architectures, which are derived from the 5 basic models shown in Table 4. Three of these basic networks *Conv*, *ResNet_1* and *ResNet_2* are convolutional and the other two *LSTM* and *GRU* are recurrent neural networks. In total, we used 14 different convolution and 8 recurrent NN models. Network architectures are shown in Figure 7.

Table 4. Networks architectures.

Layer	Conv	ResNet_1	ResNet_2	LSTM	GRU
1	conv 3x32	conv 3x32	conv 3x16	lstm	gru
2	conv 3x64	residual block 32	residual block 16	fc 2	fc 2
3	conv 3x64	residual block 32	residual block 16		
4	conv 3x128	conv 3x64	conv 3x32		
5	flatten	residual block 64	residual block 32		
6	fc 2	residual block 64	residual block 32		
7		conv 3x64	conv 3x64		
8		residual block 64	residual block 64		
9		residual block 64	residual block 64		
10		conv 3x128	conv 3x128		
11		residual block 128	residual block 128		
12		residual block 128	residual block 128		
13		flatten	flatten		
14		fc 2	fc 2		

**Figure 7.** On the left - convolutional neural network architecture *Conv*, in the middle - the scheme of the residual block of the network *ResNet* and on the right - the architecture of the recurrent neural network *LSTM*.

Since the input data is one-dimensional, all CNN architectures contain only one-dimensional convolution with a kernel of size 3. In the case of residual blocks, we combine two such one-dimensional convolutions. Each convolution layer is followed by a ReLU activation function. For *ResNet_1* and *ResNet_2*, the same types of convolution layers are used, differing only in size. The first number of the convolution layer in Table 4 expresses the size of the kernel and the second number, the number of outputs. Also, the number of outputs per layer expresses the number in the residual block. The *flatten* layer arranges the output of the previous layer into a vector, and the fully connected layer has 2 outputs, one representing a healthy and one a diseased cell.

For convolutional networks, we also used the regularization parameter dropout [20]. For *Conv* network, dropout follows after the convolution layer (activated by the ReLU function) and for *ResNets* architectures, dropout follows after the residual block unless otherwise stated. In Table A4 the dropout values for the 3 basic CNN models are marked, as well as which layers of the respective network followed.

For both recurrent networks, the values of two parameters were changed : the number of neurons and the size of the time window, that is the length of the sequence for the learning. Time window of 64 and 128 and a number of neurons of 64 and 256 were used. For dataset *A20a_B20a* we trained networks for all combinations of values of these parameters, that is 4 *LSTM* and 4 *GRU* networks. There were 20 augmentations in these experiments. For the 128 time window, both neuron counts, and both recurrent networks, we repeated the experiments with 100 augmentations.

3.4. Network training and hyperparameters

ADAM training algorithm [21] was used in all experiments. We minimize the loss function:

$$MSE = \frac{\sum_{i=1}^n (y_i - \hat{y}_i)^2}{n}, \quad (2)$$

where y_i are the required values, \hat{y}_i are the predicted values and n is the size of the dataset. Model training lasts 100 epochs, unless otherwise stated. Cyclical learning rate [22] with a period of 7 that takes on the following values was used: $(1 \cdot 10^{-3}, 1 \cdot 10^{-3}, 1 \cdot 10^{-4}, 1 \cdot 10^{-4}, 1 \cdot 10^{-4}, 1 \cdot 10^{-5}, 1 \cdot 10^{-5})$. The weights were initialized by the *xavier uniform* method [23], the bias was set to 0, and the minibatch size was 256 [24]. The parameters used for regularization have the following values: $L_1 = L_2 = 1 \cdot 10^{-3} \cdot \text{learning rate}$, for the respective values of the cyclical learning rate. The dropout setting is described above.

3.5. Technological and computational tools

Models are implemented using PyTorch [25] and trained on the NVIDIA GeForce GTX 1080 Ti graphical processing unit. Source codes are available online in the git repository: https://github.com/katkaj/rbc_classification

4. Results

More than 100 classification experiments were performed to obtain the most efficient model possible. Network design and input data selection were also optimized (section 4.1). In the following sections, we compare the accuracy of optimal models concerning the following parameters:

- the selection of extremal points (input data),
- rigidity of diseased RBCs,
- ratio of the healthy and the diseased cells in training and test data,
- margination rate of diseased cells in training data.

These parameters are used as validation criteria of the optimal model(s), and also to find out what differences in training and testing data the model can handle. (That is, to determine when it still achieves sufficient accuracy.) Insufficient accuracy of classification can also indicate shortcomings in the simulation data.

The accuracy of classification on individual (training and test) datasets is expressed in percentage as a weighted average of the accuracy of classification of healthy RBCs and the accuracy of classification of diseased RBCs.

In the Appendix in Tables A5, A6 and A7 we list the datasets that were used in the experiments for each evaluation.

284 4.1. Comparison of model accuracy with respect to input data selection and neural network 285 architecture

286 In Table 5, the accuracy of experiments that use the positions of cell centers as
287 the input, and experiments that use the positions of cell extremal points is compared.
288 In the latter, we include all experiments in which any type of information about the
289 position of extremal points (listed in Section 3.2) is used. All 9 datasets that were used
290 for classification based only on the centre of cells, were also used for classification based
291 on the extremal points. The list of datasets used in this evaluation, the number of
292 experiments performed, and the neural network architectures used for these datasets
293 are given in Table A5.

Table 5. An overview of classification experiments and their accuracy with respect to the choice of input data.

Input data	Centre position	Extremal points positions
Number of datasets	9	20
Number of experiments	61	55
The total number of used NN models	22	5
Of these, the number of basic NN architecture	5	5
Average overall training accuracy	93.79%	100%
Average training accuracy of healthy cells	98.96%	100%
Average training accuracy of diseased cells	74.02%	99.99%
Average overall testing accuracy	80.74%	98.96%
Average testing accuracy of healthy cells	94.15%	99.64%
Average testing accuracy of diseased cells	41.02%	96.25%

294 From the average testing accuracies given in Table 5, we see that it makes sense to
295 use classification based on the extremal points of cells. Models that used only cells centre
296 positions were generally unable to classify diseased cells. The most accurate model
297 classified them only with an accuracy of 70.19%.

298 4.1.1. Comparison of the efficiency of used neural networks models

299 Several neural network architectures were used for classification from cell centre
300 positions. In this case the choice of network architecture did not significantly affect the
301 accuracy of the model.

302 In the case of classification from *xyz*-coordinates of all extremal cell points and cell
303 centers, we used 5 different neural network architectures for one dataset *Be20a_Ae20a*:
304 *Conv_4d001*, *ResNet_1_4d001*, *Resnet_2*, *LSTM* and *GRU*. *Conv_4d001* network achieved
305 the best performance, as shown in the graphs in Figure 8. It has reached 100% accuracy
306 already in the 10 th epoch. In all other experiments where cell extremal points entered
307 only this network was used.

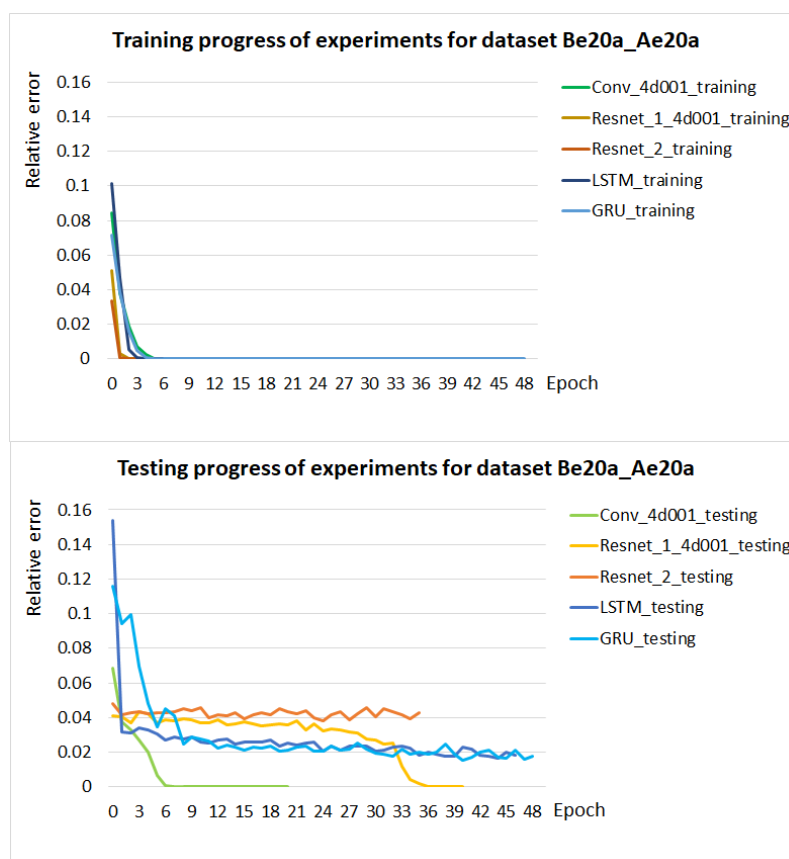


Figure 8. Training and testing progress of models for 5 different network architectures during 50 training epochs. The progress of the experiments is shown as the relative error of the accuracy of the experiments in the individual epochs.

308 4.1.2. Comparison of model accuracy with respect to the choice of extremal points

309 For the *Be20a_Ae20a* dataset, *Conv_4d001* network for 11 different selections of
 310 extremal points as NN input data was tested. We chose the positions of all 6 extremal
 311 points in all directions (with or without the centre of the cell), four extremal points for
 312 all 3 coordinate planes xy , xz , yz in all directions (with or without the centre of the cell)
 313 or four extremal points only in the direction of the selected planes (without the centre of
 314 the cell). All experiments achieved 100% accuracy in both the training and the testing
 315 phases.

316 Furthermore, when selecting 4 extremal points, we have limited ourselves to the
 317 coordinates in which we select the extremal points. From this choice of extremal points,
 318 we can obtain the described rectangle of the 2D cell image. The reason for this choice is
 319 to detect cells from the video.

320 For 7 different datasets, experiments using all 6 extremal points in all directions
 321 (hereinafter referred to as *cuboid*) and 4 extremal points in 2 directions for all 3 coordinate
 322 planes (hereinafter referred to as xy , xz a yz) were performed. The overall accuracy of
 323 their testing is given in Table 6.

324

Table 6. The overall accuracy of the testing model with the *Conv_4d001* network architecture with respect to the selection of the training and testing dataset and the choice of input data, and the average of the overall testing accuracy of the given experiments with respect to the selection of the input data.

Dataset	Choice of extremal points			
	cuboid	xy	xz	yz
Be20a_Ae20a	100%	100%	100%	100%
A40a_Ae40a	92.84%	98.51%	98.73%	98.63%
Be20a_D20a	100.00%	100.00%	99.96%	100.00%
A20b_Ae20b	97.53%	99.47%	98.90%	98.29%
A20b_D20b	99.16%	99.46%	99.66%	98.82%
Ae20b_D20b	98.91%	99.62%	99.79%	98.66%
Ae20b_A20b	98.42%	99.85%	99.41%	98.03%
Average of the overall testing accuracy	98.12%	99.56%	99.49%	98.92%

325 The differences in the accuracy of the experiments depending on the choice of
 326 extremal points are minimal. The use of extremal points in the coordinate planes *xy* and
 327 *xz* was the most advantageous. This result is expected because the blood flows in the
 328 direction of the *x* axis and therefore the elongation of the elastic blood cell is greatest in
 329 this direction.

330 The graph in Figure 9 compares the test progress of 12 experiments. They use 3
 331 various datasets and 4 extremal point selections as in the Table 6.

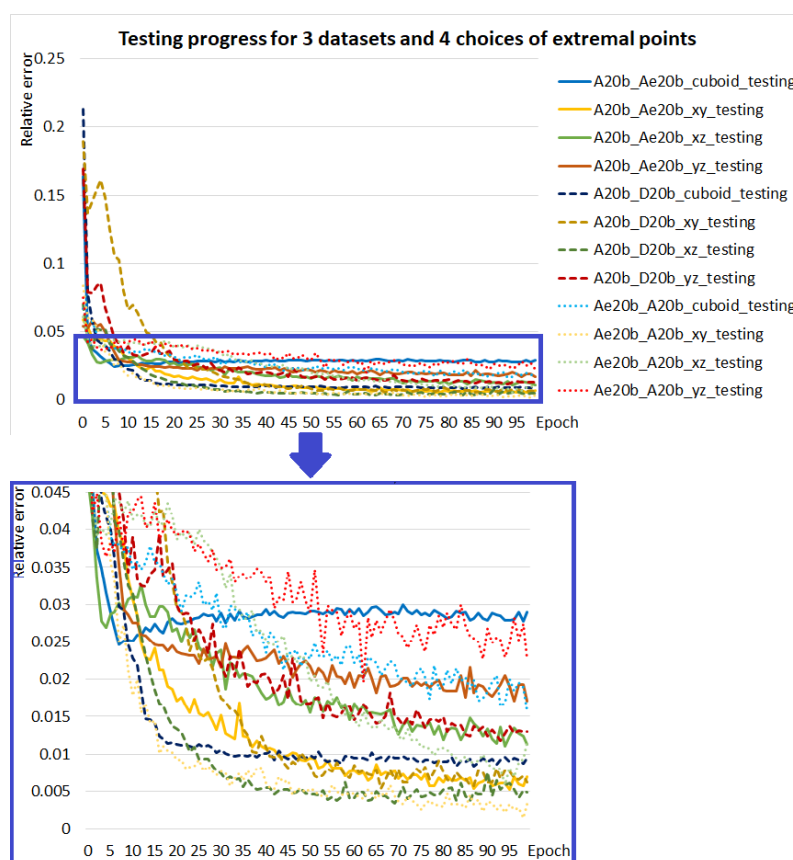


Figure 9. Testing progress of models for datasets: *A20b_Ae20b* (solid line), *A20b_D20b* (dashed line) and *Ae20b_A20b* (dotted line) and for each of them for input selections: *cuboid* (blue curves), *xy* (yellow curves), *xz* (green curves) and *yz* (red curves). The bottom graph is an enlargement of the selected area of the top graph.

4.2. Comparison of the accuracy of the model with respect to the rigidity of diseased cells

In this and the following sections, only relevant experiments are selected, to evaluate the accuracy of the models. We select them for optimal models, i.e. for models with network architecture *Conv_4d001* and with input data of *cuboid*, *xy*, *xz* or *yz* choices of extremal points. If necessary, the selection of experiments is specified in each section.

As mentioned above, we used 3 types of rigid (diseased) cells, which vary in the simulations by different settings of the stretching coefficient of the RBC. In Table 7, the average accuracy of experiments with respect to the elasticity of diseased blood cells in a dataset is compared. For the dataset *Be20a_Ae20a*, which uses the most rigid RBC with the value of the stretching coefficient $k_s = 1$, 12 experiments were performed (which turned out equally well with 100% accuracy in training and testing) and for others datasets, at most 4 experiments were performed. In this comparison only 4 experiments for dataset *Be20a_Ae20a* are included. In comparison, there are all experiments from section 4.1.2 and 2 experiments with the dataset *A20C_Ae20c*.

Table 7. Overview of classification experiments and their accuracy with respect to the rigidity of diseased cells.

Stretching coefficient k_s	1	0.3	0.03
Number of datasets	15	4	1
Number of experiments	25	16	2
Average overall training accuracy	100%	99.99%	99.99%
Average training accuracy of healthy cells	100%	100%	100%
Average training accuracy of diseased cells	100%	99.97%	99.97%
Average overall testing accuracy	99.36%	99%	91%
Average testing accuracy of healthy cells	99.36%	99.9%	99.9%
Average testing accuracy of diseased cells	99.35%	99.66%	55.54%

From the results in Table 7 we see that for $k_s = 0.3$ and $k_s = 1$ the models achieve comparably accurate results. For the most rigid cells ($k_s = 1$), the classification was 100% accurate for some datasets. For $k_s = 0.3$, the accuracy was never 100%, however, the worst testing accuracy was 97.53%. For the least rigid cells ($k_s = 0.03$), the network learned to classify diseased cells, but could not recognize them in the test dataset. These cells are more elastic and thus more similar to healthy RBCs. The data from these simulations did not show a characteristic feature for damaged cells - margination. Therefore, it is not surprising that the network cannot distinguish them so well.

4.3. Comparison of model accuracy with respect to different ratios of healthy and diseased cells in training and test data

For the most rigid type of diseased blood cells, we have datasets with 20%, 40% and 60% of diseased RBCs. We performed 6 experiments where the network was trained and tested on datasets with different ratios of healthy and diseased cells. We used 3 datasets, each with a different ratio of healthy and diseased cells, which we alternated for training and testing, see Table A6. Networks were trained using the x, y coordinates of the positions of extremal points of cells in the xy plane. For all the experiments, the trained network was able to very accurately classify the RBCs on the test set. The average accuracy of total testing is 99.6%, with the worst result of total testing being 98.78% for a network that trained on data with 20% diseased blood cells and tested on data with 40% diseased blood cells. Based on these results, we can say that the different ratio of healthy and diseased blood cells in the training and testing data does not affect the accuracy of the model. A comparison of the performed experiments is in the graphs in Figure 10. Note, that we did not train up to 100 epochs in experiments that achieved accuracy 100% on the test set.

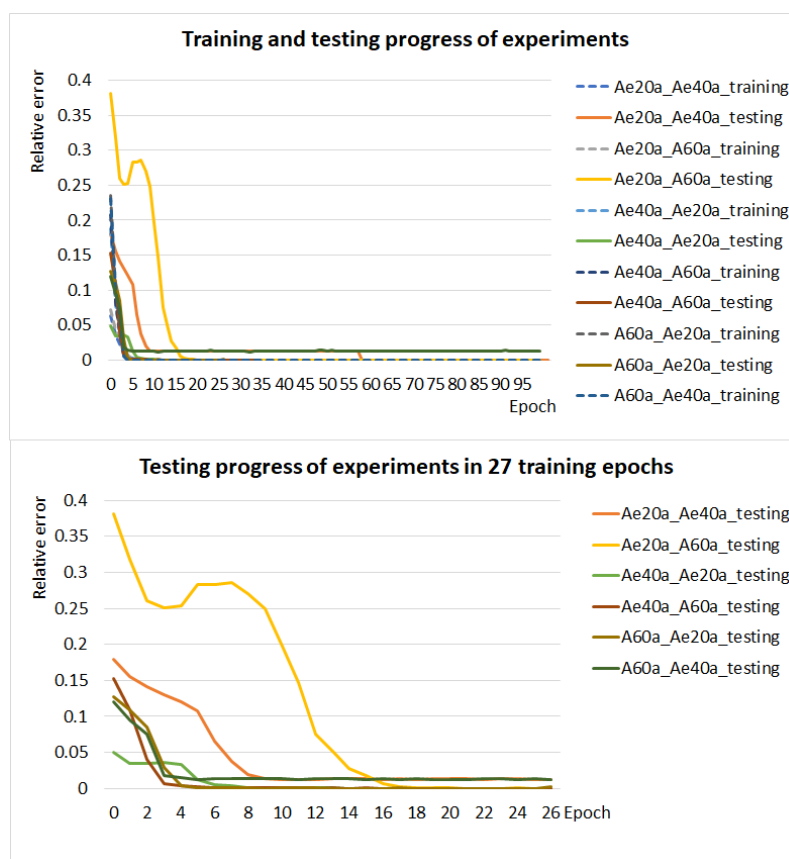


Figure 10. The graph in the figure above shows the training (dashed line) and testing (solid line) progress of six experiments with different ratios of healthy and diseased cells in the training and test dataset. The graph in the figure below compares the test progress of these experiments in 27 learning epochs.

370 4.4. Comparison of the accuracy of the model with respect to the margination of diseased cells in 371 training data

372 For 3 datasets, the network was trained on data from the (beginning) of the sim-
373 ulation, where margination of diseased blood cells did not occur or was minimal, and
374 we tested it on data that was sufficiently marginalized. An overview of datasets is in
375 Table A7. These experiments aim to determine whether the model can distinguish cell
376 damage without being able to learn their characteristic behaviour, i.e. margination.
377 For each dataset, 4 experiments were performed with extremal point choices as shown
378 in Table 6. The average overall accuracy of testing is 98.33%, which is approximately
379 1.21% less than for 4 selected datasets in which training data is marginalized, see Table 8.
380 For comparison, experiments with marginalized training data were selected, where the
381 networks trained on the same choice of positions of cell extremal points as for datasets
382 with training data without margination. The classification is the most accurate for the
383 input where the positions of xy or xz extremal point are used (see section 4.1.2). The
384 average overall testing accuracy is 99.12% for training data from experiments without
385 margination and 99.83% for training data from experiments with margination. The
386 difference between them has narrowed to 0.71%. From these results, we conclude that
387 information about margination in training data does not significantly affect the accuracy
388 of the classification of healthy and diseased blood cells.

Table 8. Accuracy of experiments with respect to margination of diseased cells in a training dataset.

Training data	Marginated	Non margined
Number of datasets	3	4
Number of experiments	12	16
Average overall training accuracy	99.99%	100%
Average training accuracy of healthy cells	100%	100%
Average training accuracy of diseased cells	99.96%	100%
Average overall testing accuracy	98.33%	99.54%
Average testing accuracy of healthy cells	99.21%	99.97%
Average testing accuracy of diseased cells	95.46%	97.81%

4.5. Discussion

From the performed experiments, the model of convolutional neural network with one-dimensional convolutional kernels achieves the best results using the x and y coordinates of cell extremal point positions in the plane xy or the x and z coordinates of cell extremal point positions in the xz plane, with blood flowing in the direction of the x axis. Thus, the network has cell position information in two dimensions. As a result, this model could have good results in classifying healthy and diseased cells from video recordings of laboratory experiments where areas in which the cells are located are detected.

The more rigid the damaged blood cells in the dataset are, the more accurately the model classifies them. For diseased blood cells with values of the stretching coefficient, $k_s = \{0.3, 1\}$, the accuracy of classification was on average 99.22%, while the worst performing experiment with optimal choice of model parameters had an accuracy of 97.53%. On data with less rigid damaged blood cells with a value of $k_s = 0.03$, the model learned to classify diseased cells, but could not recognize them in the test data. On the other hand, the data from these simulations did not show the margination that is characteristic of rigid cells.

The experiments also show that the trained network classifies blood cells on datasets with a different ratio of diseased cells with sufficient accuracy (on average with 99.6% accuracy from the performed experiments at 20%, 40% and 60% representation of diseased cells in the hematocrit). The results of experiments where the network is trained on data that are not marginalized suggest that information about margination does not significantly affect the accuracy of the classification of healthy and diseased blood cells.

Furthermore, the models are sufficiently accurate if they have information about the extremal points of the cells and, conversely, if they only have information about the positions of the centre of the cell, they usually are unable to distinguish diseased cells sufficiently. These findings support the hypothesis that the model distinguishes blood cells based on their shape rather than their trajectory.

The average overall accuracy of testing experiments with the optimal model and datasets with the stretching coefficient of at least 0.3 is 99.46%, where all values are from the interval $\langle 97.53\%, 100\% \rangle$.

5. Conclusions

The motivation for this work was the applications of computational methods to experimental blood flow data for diagnostic purposes. We show the main methods of numerical modelling of microfluidic devices that are used for the identification and separation of diseased cell from blood flow.

The simulation model and its parameters can be correctly set only when the flow from the biological and the computational experiment can be compared. Since any simulation model is only an approximation of a real biological experiment, it is not

possible to compare individual cells but it is necessary to compare the bulk, statistical properties and behaviour of the cells.

Linear models can describe some of the characteristics of the blood flow and they can be used to compare these characteristics with statistics obtained from the simulation model. However, there is usually only 2D video recording or photo available for real biological experiment processing.

This leads to important questions. How similar is the video recording of the experiment compared to the real experiment? How much information about the experiment can be obtained from 2D recording. How much information is lost and how does it affect diagnostic results.

The answers to the questions about the statistical comparison of experiments were developed in the following works [7–9]. Questions about the application of computational methods for diagnostic purposes are covered in this paper.

Neural networks were used for the identification of diseased cell. The models classify RBCs based on the time sequences of their positions. 116 experiments were performed with various neural network architectures. We used different ratios of the diseased and healthy blood cell, different types of diseased cells and different ranges of input information about individual cells. The result is a complex comparison of the effectivity of the neural network use for this classification problem. The tables show how individual settings influence the overall diagnostic success. These results can be interpreted as the rate of difference in solving this problem in a situation where we have data from video recording or more complex data from the simulation.

Further research can ponder the effectiveness of the neural network in cases when the input dataset is damaged. The question is if the neural network will be able to learn future behaviour of the simulation even in the cases when it will receive no information about this behaviour. We focused on diagnostics of the disease that manifests with more rigid RBC. If we could obtain information about the typical manifestation of other diseases in blood cell behaviour, we could focus on their diagnostics. However, neural networks allow for diagnostics of diseases of which we have no prior knowledge of how they manifest in blood cell behaviour. Then it will become a problem of explainability if we will be able to not only diagnose these diseases but also recognize them on a cellular level.

Author Contributions: Conceptualization, K.Ba., H.B. and M.Ch.; methodology, M.Ch. and K.Bu.; software, M.Ch. and K.Bu.; validation, M.Ch., K.Bu. and M.S.; formal analysis, K.Bu.; investigation, K.Bu. and M.S.; resources, M.S. and M.Ch.; data curation, M.S. and M.Ch.; writing—original draft preparation, K.Bu. and K. Ba.; writing—review and editing, H.B., K.Ba., A.B., M.Ch. and M.S.; visualization, K.Bu.; supervision, K.Ba.; project administration, K.Ba.; funding acquisition, K.Ba. All authors have read and agreed to the published version of the manuscript.

Funding: This research was funded by Operational Program "Integrated Infrastructure" of the project "Integrated strategy in the development of personalized medicine of selected malignant tumor diseases and its impact on life quality", ITMS code: 313011V446, co-financed by resources of European Regional Development Fund.

Institutional Review Board Statement: Not applicable.

Informed Consent Statement: Not applicable.

Data Availability Statement: The data used in this study are freely available in the GIT repository: https://github.com/katkaj/rbc_classification/tree/master/data.

Conflicts of Interest: The authors declare no conflict of interest.

Abbreviations

The following abbreviations are used in this manuscript:

CIF	Cell in Fluid, Biomedical Modeling & Computation Group
CNN	Convolutional neural network
GRU	Gated recurrent unit
LSTM	Long Short-Term Memory network
NN	Neural network
RBC	Red blood cell
ResNet	Residual neural network
RNN	Recurrent neural network

Appendix A

Table A1. Elastic parameters of the RBCs model coefficients used in simulation experiments in SI units.

Parameter	healthy RBC	diseased RBC (a)	diseased RBC (b)	diseased RBC (c)
Radius	$3.91\mu m$	$3.91\mu m$	$3.91\mu m$	$3.91\mu m$
Stretching coefficient k_s	$5 \cdot 10^{-3} mN/m$	$1.0 mN/m$	$3 \cdot 10^{-1} mN/m$	$3 \cdot 10^{-2} mN/m$
Bending coefficient k_b	$3 \cdot 10^{-18} Nm$	$1 \cdot 10^{-15} Nm$	$1 \cdot 10^{-17} Nm$	$1 \cdot 10^{-17} Nm$
Local area conservation k_{al}	$2 \cdot 10^{-2} mN/m$	$1.0 mN/m$	$1 \cdot 10^{-2} mN/m$	$1 \cdot 10^{-2} mN/m$
Global area conservation k_{ag}	$7 \cdot 10^{-1} mN/m$	$1.0 mN/m$	$7 \cdot 10^{-1} mN/m$	$7 \cdot 10^{-1} mN/m$
Volume conservation k_v	$9 \cdot 10^{-1} kN/m^2$	$1.0 kN/m^2$	$9 \cdot 10^{-1} kN/m^2$	$9 \cdot 10^{-1} kN/m^2$

Table A2. Numerical parameters of fluid used in simulations.

Parameter	SI Units
LB-grid for fluid	$1 \cdot 10^{-6} m$
Density	$1.025 \cdot 10^3 kg/m^3$
Kinematic viscosity	$1.3 \cdot 10^{-6} m^2/s$
Friction coefficient (ξ)	$1.41 [-]$

Table A3. Overview of simulation experiments.

Rigidity of diseased RBC	The ratio of diseased RBCs	The total number of time records	Name
a	20%	597	$A20a$
a	20%	698	$Ae20a$
a	20%	733	$B20a$
a	20%	990	$Be20a$
a	20%	724	$C20a$
a	40%	189	$A40a$
a	40%	717	$Ae40a$
a	60%	706	$A60a$
b	20%	603	$A20b$
b	20%	1402	$Ae20b$
b	20%	945	$D20b$
c	20%	735	$A20c$
c	20%	1466	$Ae20c$

Table A4. Overview of used dropouts and number of augmentations for basic models of convolutional networks used for the classification experiment.

Dropout	Suffix in the name	Conv	ResNet_1	ResNet_2
0 no dropout		✓	✓	✓
0.5 after the last convolutional layer	<i>d05</i>	✓	✓	✓
0.5 after each convolutional layer	<i>4d05</i>	✓	✓	✓
0.2 after each convolutional layer	<i>4d02</i>	✓	✓	—
0.01 after each convolutional layer	<i>4d001</i>	✓	✓	—
0.01 between each convolution and the residual block	<i>4d001_beforeResBlock</i>	—	✓	—

481 The suffix column in the name specifies the appendix after the base network name.
 482 For example, a Conv network with a 0.5 dropout after the last convolution layer is named
 483 *Conv_d05*. Thus, we obtained 14 of various CNN models (marked with a tick), which
 484 were used to solve the classification problem.

Table A5. An overview of datasets used to compare the accuracy of the model with respect to the choice of input data and the architecture of the neural network.

Dataset	Cell centre position		Cell extremal points positions		
	Number of experiments	Number of network architectures	Number of experiments	Number of network architectures	Number of selections of input data
A20a_B20a	33	22	1	1	1
B20a_A20a	5	5	1	1	1
Ae20a_Be20a	4	4	1	1	1
Be20a_Ae20a	4	4	16	5	12
B20a_Ae20a	—	—	1	1	1
B20a_Be20a	—	—	1	1	1
Be20a_C20a	—	—	4	1	4
A40a_Ae40a	1	1	4	1	4
A20a_A40a	11	11	1	1	1
Ae20a_Ae40a	—	—	2	1	2
Ae20a_A60a	—	—	1	1	1
Ae40a_Ae20a	—	—	1	1	1
Ae40a_A60a	—	—	1	1	1
A60a_Ae20a	—	—	1	1	1
A60a_Ae40a	—	—	1	1	1
A20b_Ae20b	1	1	4	1	4
Ae20b_A20b	—	—	4	1	4
A20b_D20b	1	1	4	1	4
Ae20b_D20b	1	1	4	1	4
A20c_Ae20c	—	—	2	1	2

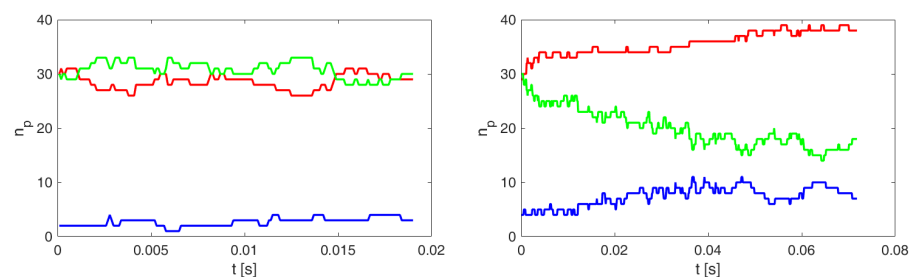
Table A6. Comparison of model accuracy with respect to different ratios of healthy and diseased cells in training and test data.

Dataset	Number of experiments
Ae20a_Ae40a	1
Ae20a_A60a	1
Ae40a_Ae20a	1
Ae40a_A60a	1
A60a_Ae20a	1
A60a_Ae40a	1

Table A7. Comparison of model accuracy with respect to the occurrence of margination of diseased cells in training and test data.

Dataset	Number of experiments
Training data without margination	
A40a_Ae40a	4
A20b_Ae20b	4
A20b_D20b	4
Training data with margination	
Be20a_Ae20a	4
Be20a_C20a	4
Ae20b_D20b	4
Ae20b_A20b	4

485 The graphs in Figure A1 show the margination of rigid cells with the value $k_s = 1$.
 486 The entire volume of the channel is divided into 3 (lengthwise) coaxial areas along the
 487 central axis of the flow: the central area of the channel (blue line), the peripheral area
 488 of the channel (red line) and the area between the peripheral and central area of the
 489 channel (green line). We monitored the radial migration of rigid cells, i.e. the level
 490 of their marginalization, by the number of their centres of mass (n_p) in the individual
 491 regions created in each recorded simulation step.

**Figure A1.** Time evolution of the number of rigid cells in the three coaxial regions for the simulation experiments A40a (left) and Ae40a (right). The red curve represents n_p in the peripheral region, the green between the peripheral and central regions, and the blue in the central region of the channel.

492 Figure 2 shows rigid cell margination with $k_s = 0.3$ for insufficiently margined
 493 training dataset A20b and for tested datasets with margined rigid cells Ae20b and
 494 D20b.

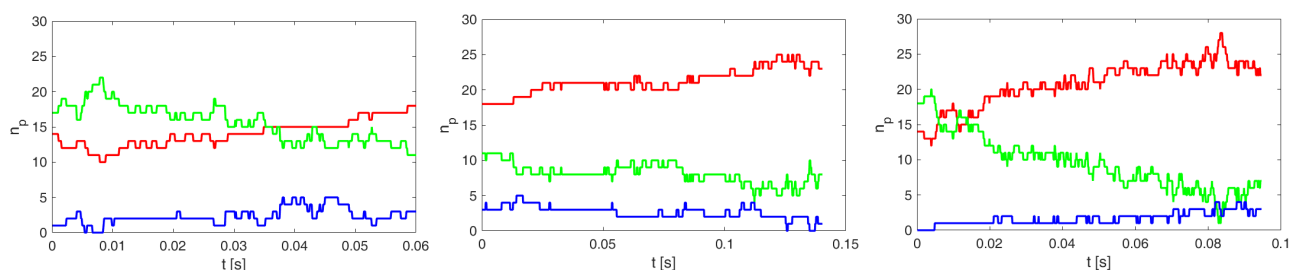


Figure 2. Time evolution of the number of rigid cells in the three coaxial regions for the simulation experiments A20b (left), Ae20b (middle) and D20b (right). The red curve represents n_p in the peripheral region, the green between the peripheral and central regions, and the blue the central region of the channel.

References

1. Mousavi Shaegh, S.A.; Nguyen, N.T.; Wereley, S. *Fundamentals and Applications of Microfluidics*; Norwood, MA : Artech House, 2019; p. 576.
2. CIF. Cell in Fluid, Biomedical Modeling & Computation Group. <https://cellinfluid.fri.uniza.sk/>. Accessed: 21/4/2021.
3. Jančígová, I.; Kovalčíková, K.; Bohiníková, A.; Cimrák, I. Spring-network model of red blood cell: From membrane mechanics to validation. *International Journal for Numerical Methods in Fluids* **2020**, *92*, 1368–1393.
4. Cimrák, I. Collision rates for rare cell capture in periodic obstacle arrays strongly depend on density of cell suspension. *Computer Methods in Biomechanics and Biomedical Engineering* **2016**, *19*, 1525–1530.
5. Gusenbauer, M.; Tothova, R.; Mazza, G.; Brandl, M.; Schrefl, T.; Jančígová, I.; Cimrák, I. Cell Damage Index as Computational Indicator for Blood Cell Activation and Damage. *Artificial organs* **2018**, *42*, 746–755.
6. Smiesková, M.; Bachratá, K. Validation of Bulk Properties of Red Blood Cells in Simulations. *2019 International Conference on Information and Digital Technologies (IDT)* **2019**, pp. 417–423.
7. Bachratá, K.; Bachratý, H.; Slavík, M. Statistics for comparison of simulations and experiments of flow of blood cells. *EPJ Web of Conferences* **2017**, *143*, 02002.
8. Bachratý, H.; Bachratá, K.; Chovanec, M.; Kajánek, F.; Smiesková, M.; Slavík, M. Simulation of Blood Flow in Microfluidic Devices for Analysing of Video from Real Experiments. *Bioinformatics and Biomedical Engineering*; Rojas, I.; Ortuño, F., Eds. Springer International Publishing, 2018, pp. 279–289.
9. Bachratý, H.; Kovalčíková, K.; Bachratá, K.; Slavík, M. Methods of exploring the red blood cells rotation during the simulations in devices with periodic topology. *2017 International Conference on Information and Digital Technologies (IDT)* **2017**, pp. 36–46.
10. Kwon, S.; Lee, D.; Han, S.J.; Yang, W.; Quan, F.; Kim, K. Biomechanical properties of red blood cells infected by Plasmodium berghei ANKA. *Journal of Cellular Physiology* **2019**, *234*, 20546 – 20553.
11. Chang, H.Y.; Yazdani, A.; Li, X.; Douglas, K.; Mantzoros, C.; Karniadakis, G. Quantifying Platelet Margination in Diabetic Blood Flow. *Biophysical Journal* **2018**, *115*.
12. Hou, H.; Bhagat, A.A.; Chong, A.; Mao, P.; Tan, K.; Han, J.; Lim, C. Deformability based cell margination — A simple microfluidic design for malaria-infected erythrocyte separation. *Lab on a chip* **2010**, *10*, 2605–13.
13. Xu, M.; Papageorgiou, D.; Abidi, S.; Dao, M.; Zhao, H.; Karniadakis, G. A deep convolutional neural network for classification of red blood cells in sickle cell anemia. *PLOS Computational Biology* **2017**, *13*, e1005746.
14. Loh, D.R.; Yong, W.X.; Yapeter, J.; Subburaj, K.; Chandramohanadas, R. A deep learning approach to the screening of malaria infection: Automated and rapid cell counting, object detection and instance segmentation using Mask R-CNN. *Computerized Medical Imaging and Graphics* **2021**, *88*, 101845.
15. Maitra, M.; Gupta, R.; Mukherjee, M. Detection and Counting of Red Blood Cells in Blood Cell Images using Hough Transform. *International Journal of Computer Applications* **2012**, *53*, 13–17.
16. Kajánek, F.; Cimrák, I. Advancements in Red Blood Cell Detection using Convolutional Neural Networks. *Proceedings of the 13th International Joint Conference on Biomedical Engineering Systems and Technologies - Volume 3: BIOINFORMATICS*, INSTICC, SciTePress, 2020, pp. 206–211.
17. Cimrák, I.; Gusenbauer, M.; Jančígová, I. An ESPResSo implementation of elastic objects immersed in a fluid. *Computer Physics Communications* **2014**, *185*, 900–907.
18. Ahlrichs, P.; Dünweg, B. Lattice-Boltzmann Simulation of Polymer-Solvent Systems. *International Journal of Modern Physics C (IJMPC)* **1998**, *09*, 1429–1438.
19. Tóthová, R.; Jančígová, I.; Bušík, M. Calibration of elastic coefficients for spring-network model of red blood cell. *2015 International Conference on Information and Digital Technologies* **2015**, pp. 376–380.
20. Srivastava, N.; Hinton, G.; Krizhevsky, A.; Sutskever, I.; Salakhutdinov, R. Dropout: A Simple Way to Prevent Neural Networks from Overfitting. *J. Mach. Learn. Res.* **2014**, *15*, 1929–1958.
21. Kingma, D.P.; Ba, J. Adam: A Method for Stochastic Optimization. *3rd International Conference on Learning Representations, ICLR 2015, San Diego, CA, USA, May 7-9, 2015, Conference Track Proceedings*; Bengio, Y.; LeCun, Y., Eds., 2015.

-
22. Smith, L. Cyclical Learning Rates for Training Neural Networks. 2017 IEEE Winter Conference on Applications of Computer Vision (WACV), 2017, pp. 464–472.
 23. Glorot, X.; Bengio, Y. Understanding the difficulty of training deep feedforward neural networks. *Journal of Machine Learning Research - Proceedings Track* **2010**, 9, 249–256.
 24. Li, M.; Zhang, T.; Chen, Y.; Smola, A.J. Efficient mini-batch training for stochastic optimization. KDD, 2014, pp. 661–670.
 25. PyTorch. <https://pytorch.org/>. Accessed: 27/1/2021.